Journal of Alloys and Compounds 508 (2010) 500–506

Contents lists available at ScienceDirect

Journal of Alloys and Compounds

journal homepage: www.elsevier.com/locate/jallcom

Effect of synthesis condition on properties of $Ce_{0.67}Zr_{0.33}O_2$ mixed oxides and its application in Pd-only three-way catalysts

Bo Zhao [a,b], Qiuyan Wang [a], Guangfeng Li [a], Renxian Zhou [a,*]

[a] Institute of Catalysis, Zhejiang University, Hangzhou 310028, PR China
[b] School of Pharmaceutical and Chemical Engineering, Taizhou University, Taizhou 317000, PR China

ARTICLE INFO

Article history:
Received 20 March 2010
Received in revised form 22 August 2010
Accepted 24 August 2010
Available online 22 September 2010

Keywords:
Ceria–zirconia
Synthesis condition
Oxygen storage capacity
Reducibility
Pd-only three-way catalyst

ABSTRACT

$Ce_{0.67}Zr_{0.33}O_2$ (CZ) mixed oxide was prepared by coprecipitation and effect of the synthesis conditions on CZ properties were investigated in this work, as well as the catalytic performance of Pd-only three-way catalyst (TWC) supported on the prepared CZ. With the increase of aging temperature during precipitation, the crystallite size of CZ increases significantly, while the oxygen storage capacity complete (OSCC) drops and no notable effect on porosity of CZ is observed. The porosity is mainly determined by drying temperature and pH value during precipitation. Prepared under optimized conditions (precipitation at the pH of 9.5, aging at 25 °C and then drying under supercritical condition in alcohol), the CZ samples exhibit good properties. This preparation procedure leads to CZ with proper pore size distribution, larger average pore size (20.42 nm), higher pore volume (0.69 cm^3/g) and enhanced OSCC value (383.0 μmol/g). Furthermore, the Pd-only TWC supported on the CZ synthesized under the optimized conditions exhibits satisfactory catalytic activity and very low reduction temperature (53 °C).

1. Introduction

Recently, environmental pollution has attracted more and more attention and especially, the exhaust from vehicle has poses significant abatement problems [1].

In response to the challenges associated with treatment of these exhaust, three-way catalyst (TWC) has been widely used to reduce pollutant emissions from gasoline engine powered vehicles [2]. Improving performance of the catalyst for the vehicle exhaust is key issue to meet the increasingly standard of emission regulations. The new generation of TWC should have the following two characteristics: (i) high thermal stability to resist high temperature sintering and deactivation resulting from the closely coupled converter; (ii) high surface area to increase the reaction efficiency, achieve higher noble metal dispersion, and thereby decrease noble metal usage [3].

The CeO_2-based material in TWC acts as a buffer against the considerable oscillations in air-to-fuel ratio with their oxygen storage and release function and guarantees a satisfactory performance of TWC [4]. Among all ceria-related materials, ceria–zirconia mixed oxides with the composition of $Ce_xZr_{1-x}O_2$ have attracted increasing interests due to their good thermal resistance to sintering and superior oxygen storage capacities (OSCs) [5–7]. Moreover, Ce-rich compositions were preferred for the purposes of catalysis and better results were obtained based on $Ce_xZr_{1-x}O_2$ with x ranging from 0.6 to 0.8 [8]. Recently, to achieve higher energy efficiency, the ratio of air/fuel fed into internal combustion engines higher than 14.7 (the stoichiometric value) is suggested. However, high ratio of air/fuel usually results in the low NO reduction efficiency of TWC in such a fuel-lean condition. Consequently, development of a new generation of TWC to improve the NO reduction activity in oxygen-rich condition poses new challenges for researchers and engineers [9]. It was found that CeO_2–ZrO_2 (CZ) solid solution favors NO reduction in the fuel-lean combustion conditions as it is able to store the excess oxygen into the bulk of the catalysts [10–12].

Generally, the properties of CZ are significantly determined by preparation process and therefore, various methods for the preparation of CZ, such as coprecipitation [13,14], hydrothermal synthesis [15], microemulsion [16], combustion synthesis [17,18] and sol–gel technique [19,20] were reported. Among these preparation methods, the coprecipitation is considered as one of the competent routes since it is relatively simple, scalable, and inexpensive [9].

Chen et al. [21] investigated the effect of calcination temperature on the crystallite growth of cerium oxide nano-powders prepared by the coprecipitation process and concluded that face-centered cubic phase crystallization was observed with calcination at temperatures from 200 °C to 1000 °C. However, the effects of other synthesis condition of coprecipitation on the properties of CZ are not clear yet. Therefore, in this study, the effects of synthesis

* Corresponding author. Tel.: +86 571 88273290; fax: +86 571 88273283.
E-mail address: zhourenxian@zju.edu.cn (R. Zhou).

0925-8388/$ – see front matter.
doi:10.1016/j.jallcom.2010.08.101

conditions on properties of $Ce_{0.67}Zr_{0.33}O_2$ prepared by coprecipitation were investigated. In addition, the effects of properties of the $Ce_{0.67}Zr_{0.33}O_2$ on the catalytic performance of Pd-only TWC were discussed as well.

2. Experimental

2.1. Catalyst preparation

$Ce_{0.67}Zr_{0.33}O_2$ was prepared by a coprecipitation route. $Ce(NO_3)_3$ and $ZrO(NO_3)_2$ were used as metal precursors and dissolved in water. The solution of aqueous ammonia was added dropwise to the solution of metal precursors under continuous stirring and the pH was controlled at certain value (pH 8.6, 9.0, 9.5, 10.0). The obtained slurry was aged at different temperature (25 °C, 40 °C, 60 °C) for 12 h. The precipitate was first filtered and washed with deionized water until no pH change could be detected and then 500 ml of alcohol was used to remove the remaining water. It was further dried under alcohol atmosphere at different temperature (170 °C, 200 °C, 230 °C, 250 °C) for 3 h and calcined at 500 °C for 4 h in air. All of the obtained supports were pressed into pellets, crushed and sieved to 40–60 meshes. The supports were labeled as CZ (pH; *A*; *T*), where pH, *A* and *T* represent pH value upon precipitation, aging temperature and drying temperature, respectively.

The Pd-only three-way catalysts with different CZ as supports were prepared by incipient impregnation method with aqueous solutions of H_2PdCl_4 as metal precursors. Pd content was 0.5 wt%. The impregnated samples were reduced using hydrazine hydrate solution for 2 h, washed several times with deionized water until no Cl^- ions detected in the filtered solution, and then dried at 110 °C for 2 h followed by calcination at 500 °C for 2 h. These as-prepared catalysts were designated as Pd/CZ (pH; *A*; *T*).

2.2. Characterization

X-ray diffraction (XRD) patterns were collected on a Rigaku D/Max-IIIB powder diffractometer using Cu Kα radiation. The working voltage of the instrument was 40 kV and the current was 40 mA. The diffraction pattern was recorded at 0.02° intervals in the range of $20° \leq 2\theta \leq 80°$.

The textural properties of ceria–zirconia mixed oxides were measured by N_2 adsorption using a Micromeritics TriStarIIapparatus. Prior to the measurement, the samples (0.15 g) were degassed at 200 °C for 2 h under vacuum. Then N_2 adsorption was carried out at the liquid nitrogen temperature.

Raman spectra were obtained with a UV-HR Raman spectrometer. The exciting wavelength was 325 nm from a He–Gd laser. Spectra consisted of two accumulations of 30 s with a resolution of 4 cm^{-1}. A frequency range of 100–1000 cm^{-1} was observed.

Oxygen storage capacity (OSC) of prepared ceria–zirconia mixed oxide was measured by pulse injection technique. The amount of oxygen consumed during the reoxidation stage was referred to as oxygen storage capacity complete (OSCC) and the measurement was carried out using CHEMBET-3000 (Quantachrome Instrument Co. Ltd., USA). The samples (0.1 g) were reduced at 550 °C for 60 min in H_2 (10 ml min^{-1}), then cooled down to 300 °C and purged with He (30 ml min^{-1}) for 30 min. A given amount of O_2 (0.15 ml) was pulsed every 5 min until the intensity of the peak reached a constant value.

Hydrogen-temperature-programmed reduction (H_2-TPR) experiment was carried out in a conventional system equipped with a thermal conductivity detector (TCD). The samples (0.05 g) were pretreated at 300 °C for 30 min and cooled down to 150 °C in air. Then the samples were further purged in flowing He (40 ml min^{-1}) for 1 h. The gas flow was then switched to 5% H_2/Ar (40 ml min^{-1}) and the temperature was raised to 900 °C at a rate of 10 °C min^{-1}. The consumption of H_2 was monitored by a TCD and the effluent H_2O formed during H_2-TPR was adsorbed with a 5 Å molecular sieve.

2.3. Catalytic activity test

Catalytic activity tests were carried out with a fixed-bed continuous flow reactor. The catalysts (0.2 ml) in a quartz tube were held by packing quartz wool at both ends of the catalyst bed. The reaction mixture containing NO (1000 ppm), NO_2 (300 ppm), C_3H_6 (670 ppm), C_3H_8 (330 ppm), CO (7500 ppm), O_2 (7450 ppm) and balance Ar was fed to the reactor at a GHSV of 43,000 h^{-1}.The concentration of CO, NO, NO_2 and total HC (C_3H_6 and C_3H_8) were analyzed by on-line Fourier transform infrared spectrophotometer (Bruker EQ55) equipped with a multiple reflection transmission cell (Infrared Analysis Inc.). All spectra were taken at a resolution of 2 cm^{-1} for 128 scans.

3. Results and discussion

3.1. XRD characterization

The X-ray diffraction patterns of synthesized CZ are shown in Fig. 1 and lattice parameters and crystallite sizes of samples are listed in Table 1. The broad peaks in Fig. 1 are attributed to the presence of small crystallites. Moreover, regardless of the synthesis conditions, the major peaks of all CZ samples are consistent with the characteristic peaks of cubic fluorite structure [22]. Table 1 reveals that the lattice parameters of cubic phase measured by XRD for all CZ samples are in the range of 0.5403–0.5409 nm, which are smaller than that of pure CeO_2 (0.5418 nm) [23]. Since the ionic radius of Zr^{4+} (0.084 nm) is smaller than that of Ce^{4+} (0.097 nm), the lattice constant of CeO_2–ZrO_2 declines with the incorporation of zirconium into the ceria unit cell [24]. According to Wang et al. [25], when large cerium ions are replaced by small zirconium ions in the lattice, a nonequivalent metal–oxygen distance is formed, producing structure distortion. Furthermore, the cationic occupancy number in the cubic structure is always smaller than 0.02083 which is present in an ideal ceria crystal. It indicates that some cationic lattice defects are created in the crystalline structure of CeO_2–ZrO_2 [25]. With the decreasing of lattice parameters for all samples, we suggest that some cationic lattice defects are also created in all of CZ samples prepared by different synthesis conditions.

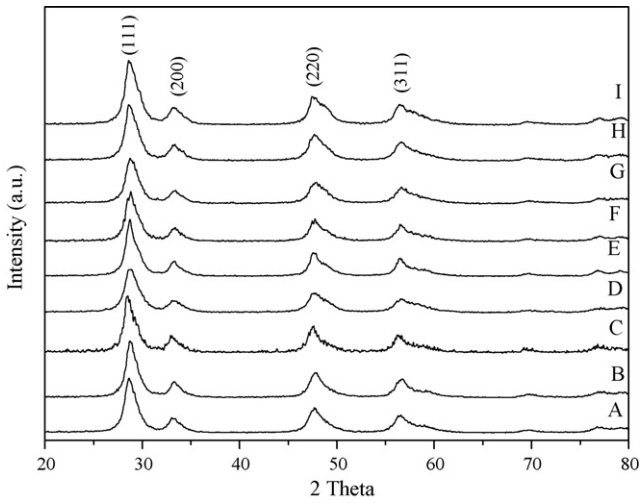

Fig. 1. XRD patterns of (A) CZ (8.6; 25; 250); (B) CZ (9.0; 25; 250); (C) CZ (9.5; 25; 250); (D) CZ (10.0; 25; 250); (E) CZ (9.5; 40; 250); (F) CZ (9.5; 60; 250); (G) CZ (9.5; 25; 170); (H) CZ (9.5; 25; 200); (I) CZ (9.5; 25; 230).

The average crystal sizes of samples are determined by the Scherrer equation (as illustrated in Table 1) and all samples are nanocrystalline. It can also be observed that the average crystallite size of the CZ prepared at the pH of 8.6 is similar as that prepared at the pH of 9.0 during precipitation. However, the crystallite size increases with aging or drying temperature during synthesis process. For example, with the drying temperature increasing from 170 °C to 230 °C, the crystallite size slightly increases from 7.1 nm to 8.1 nm. Moreover, it is worth mentioning that the increasing of aging temperature from 25 °C to 60 °C results in the increase of

Table 1
Lattice parameters and crystallite sizes of CZ samples prepared by different synthesis conditions.

Sample	Lattice parameter (nm)	Unit cell volume (nm^3)	Crystallite size (nm)
CZ (8.6; 25; 250)	0.5403	0.1577	6.7
CZ (9.0; 25; 250)	0.5405	0.1579	6.7
CZ (9.5; 25; 250)	0.5407	0.1581	7.9
CZ (10.0; 25; 250)	0.5406	0.1580	7.6
CZ (9.5; 40; 250)	0.5409	0.1584	10.3
CZ (9.5; 60; 250)	0.5408	0.1582	11.4
CZ (9.5; 25; 170)	0.5408	0.1578	7.1
CZ (9.5; 25; 200)	0.5408	0.1579	7.6
CZ (9.5; 25; 230)	0.5407	0.1580	8.1

Table 2
BET surface area (S), total pore volume (V) and average pore diameter (D) of different CZ samples.

Sample	S (m^2/g)	V (cm^3/g)	D (nm)
CZ (8.6; 25; 250)	102.3	0.67	21.66
CZ (9.0; 25; 250)	95.9	0.64	22.54
CZ (9.5; 25; 250)	105.0	0.69	20.42
CZ (10.0; 25; 250)	148.5	0.72	15.63
CZ (9.5; 40; 250)	106.1	0.82	23.07
CZ (9.5; 60; 250)	102.7	0.76	22.75
CZ (9.5; 25; 170)	107.8	0.40	11.31
CZ (9.5; 25; 200)	111.0	0.44	12.56
CZ (9.5; 25; 230)	129.6	0.63	15.44

crystallite size from 7.9 nm to 11.4 nm. This result indicates that the crystallite growth of the CZ is significantly affected by aging temperature rather than by drying temperature.

3.2. N_2 adsorption–desorption measurements

Table 2 presents the BET surface area, pore volume and average pore diameter of different CZ samples. BET areas range from 95.9 m^2/g to 148.5 m^2/g with most of the samples at 105.0 ± 5 m^2/g. The surface area of the solid solution prepared by drying under alcohol atmosphere is approximate 10–15% higher than that prepared by other groups using coprecipitation methods [9]. It is well known that during the precipitation stage, water molecules occupy the internal pores to forming hydrous metal oxides. Following drying process, the capillary pressure at the liquid–vapor interface in the pores produces stress on the metal oxide framework, thus provoking the collapse of the pore network and in turn, reducing their surface area. The capillary pressure in the pores is generally proportional to the surface tension and the presence of the alcohol can reduce water surface tension in the pores and the shrinkage degree of dried precipitations. Therefore, relative high surface area can be obtained by using the method of drying under alcohol atmosphere. The pore volumes of CZ samples prepared at different pH or aging temperatures are generally high (>0.64 cm^3/g). In addition, a direct correlation between the drying temperature and the pore volume can be seen. With the drying temperature increasing from 170 °C to 250 °C, the pore volume increases from 0.40 cm^3/g to 0.69 cm^3/g.

The pore size distribution of different CZ samples is presented in Figs. 2–4. Fig. 2 demonstrates that the sample prepared at pH between 8.6 and 9.5 exhibits similar pore diameter and pore volume. However, with further increasing of pH, the average mesopore size shifts to lower value and it decreases to 15.63 nm for the CZ (10.0; 25; 250). The surface area usually varies according to pore diameter and volume. The relationship between the surface area (S) and the pore radius (R_p) with the total pore volume can be expressed as follows: $S = f(V_p/R_p)$ [9]. One may find from Table 2 that the surface area is 102.3, 95.9 and 105.0 m^2/g for the sample prepared at the pH of 8.6, 9.0 and 9.5, respectively. This variation of surface area is not evident because the pore diameter and pore volume remain almost the same within this pH range. However, with the pH increasing to 10.0, the surface area of CZ increases to 148.5 m^2/g, which may be resulted from the obvious decrease of pore diameter.

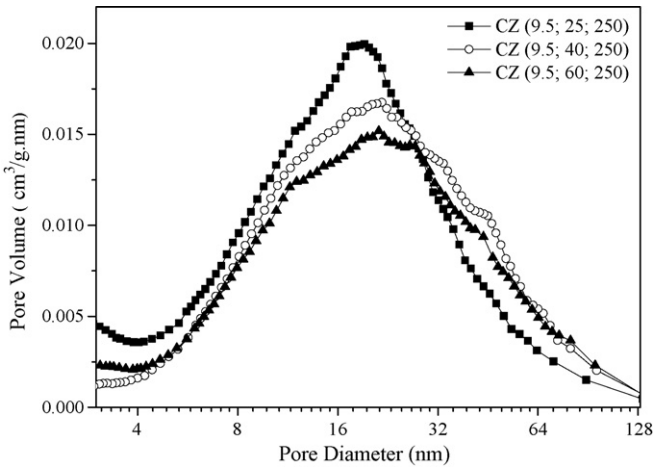

Fig. 3. Pore size distribution of CZ prepared by different aging temperature.

Figs. 3 and 4 show a progressive modification of pore size distribution for samples prepared at different aging or drying temperature. The mean pore diameters of all samples increase with increasing temperature. In addition, the differences between samples prepared at different aging temperatures are not as notable as those of samples prepared at different drying temperatures. Moreover, CZ (9.5; 40; 250) and CZ (9.5; 60; 250) samples share the similar texture with almost the identical average pore diameter and surface area. By contrast, Fig. 4 shows that with the increasing of drying temperature, the pore size distribution becomes much wider, together with the increase of average pore size. For the sample dried at 250 °C, the average pore size is 20.42 nm, which is significantly larger than those of samples dried between 170 °C and 230 °C. The supercritical point of alcohol is 241 °C and 6.38 MPa and

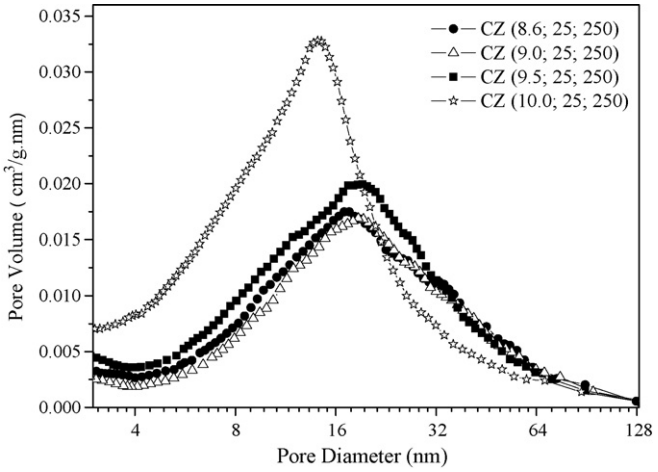

Fig. 2. Pore size distribution of CZ prepared by different pH.

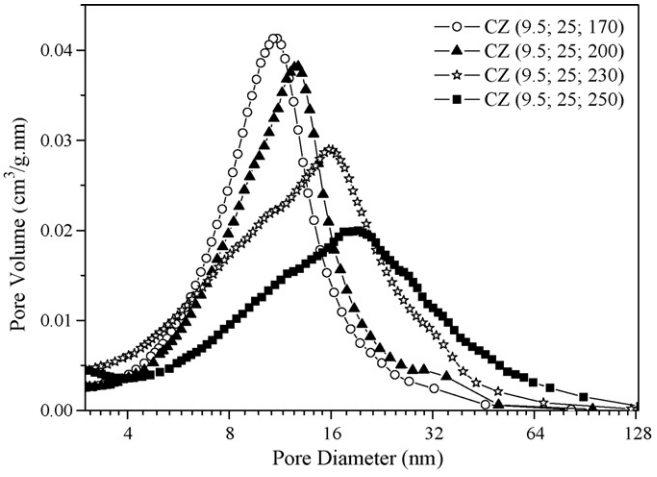

Fig. 4. Pore size distribution of CZ prepared by different drying temperature in alcohol.

therefore, the precipitates dried at 250 °C (7.5 MPa) is under supercritical condition, which subsequently results in relatively large pore size and pore volume of CZ. The textural properties such as surface area, pore volume and mean pore diameter play an important role in the performance of catalytic supports, especially at high space velocity such as those of TWC, which requires the supports to have proper surface area, pore volume and proper pore diameter distribution [26]. Furthermore, pore distribution of support material is also the key property for diffusion in heterogeneous catalysis [27]. Consequently, as discussed afterwards in the context of catalytic activity, CZ samples dried under supercritical condition in alcohol should be more suitable as catalytic support for TWC.

3.3. Raman characterization

In contrast to XRD, which allows determining just cation sublattice symmetry, Raman spectroscopy technique is able to get information about oxygen anions position [28]. As Fig. 5 shows, Raman spectra of the as-prepared samples are quite similar and have strong absorption bands at around 452 cm^{-1} and 620 cm^{-1}. The spectra also display a low intensity band at around 316 cm^{-1}. Theoretically, only one F_{2g} mode centered at ca. 490 cm^{-1} is Raman active for the cubic fluorite structure (space group $Fm3m$ CeO_2) [29]. Literatures show that in the Raman spectrum of ceria–zirconia, which also has a fluorite structure, the F_{2g} mode is centered at 452–456 cm^{-1} [10,30,31]. Therefore, the intense absorption observed at 452 cm^{-1} can be assigned to the F_{2g} vibration of the fluorite-type lattice of CZ solid solution. It can be considered as a symmetric breathing mode of the oxygen atoms around cerium ions. The broad bands at about 620 cm^{-1} are ascribed to oxygen vacancies in the CeO_2 lattice and attributed to the presence of defective structure in CeO_2–ZrO_2 materials induced by introducing Zr into the fluorite structure of CeO_2 [32]. The appearance of weak bands at about 316 cm^{-1} can be attributed to a partial breaking of $Fm3m$ symmetry due to a tetragonal displacement of oxygen atoms from their ideal fluorite lattice positions [33,34]. Such a spectral feature is attributed to the presence of a t″ phase. Some authors [31] suggest that three phases with space group P42/nmc (t, t′, and t″) may exist in CZ which is depended on preparation method and Ce content. Phase t is the most stable and obtained by diffusion and decomposition; t′ phase is formed by transition without diffusion. Finally, t″ is an intermediary phase between t′ and the cubic structure. It shows $c/a = 1$, which means that the cation in t″ phase is in the cubic position, but an oxygen ion is displaced from the ideal fluorite site. Some authors suggest phases t, t′ and t″ for Ce between 20–40%, 40–65% and 60–80%, respectively [31,35]. Our XRD results do not show the formation of t″ phase for CZ samples. On the contrary, Raman spectroscopy results and some work in literatures suggest the presence of t″. Since the lattice cations are the species that most contribute to the X-ray diffraction result, it is inferred that XRD is not sensitive to oxygen displacements from ideal lattice positions and may be unable to detect the small differences between t″ and cubic structures. It is exactly the key feature which makes the distinction between the cubic and t″ tetragonal structures. This apparent contradiction has already been addressed by other research groups [31].

3.4. OSCC measurements

OSCC values of $Ce_{0.67}Zr_{0.33}O_2$ samples measured at 300 °C are illustrated in Fig. 6. It has been reported that oxygen vacancies exist in the ceria–zirconia solids, which may function as oxygen buffer to store oxygen species [36]. As suggested by Cho [37], in the OSC measurement by the pulse method, the oxygen uptake is controlled by the mobility of oxygen at a given temperature rather than by the ultimate oxygen-storage capacity of the support, which is in fact independent of the temperature. Based on the results of Fig. 6, we suggest that preparation conditions of CZ have influence on the capacity of its storing oxygen. For the samples prepared at different pH, their O_2-uptake order is as follow: CZ (9.5; 25; 250) > CZ (9.0; 25; 250) > CZ (8.6; 25; 250) ≫ CZ (10.0; 25; 250), indicating that the optimum pH value is 9.5. Similarly, the preparation step of aging plays an important role in the properties of CZ solid solutions. For example, the OSCC decreases from 383.0 μmol/g to 361.8 μmol/g when the temperature increases from 25 °C to 60 °C. In addition, according to Table 2 and Fig. 6, it should be pointed out that the OSCC has no direct correlation with surface areas. The same phenomenon has also been observed by Mamontov et al. [38].

3.5. Temperature-programmed reduction

Figs. 7–9 present H_2-TPR profiles of different Pd/CZ catalysts. It can be seen that all of the catalysts exhibit one or two dominant lower temperature reduction peak. Previous investigations have reported that palladium oxide is reduced to palladium metal at 60–90 °C for Pd/Ce-Zr-O catalysts [39]. Thus, we suggest that

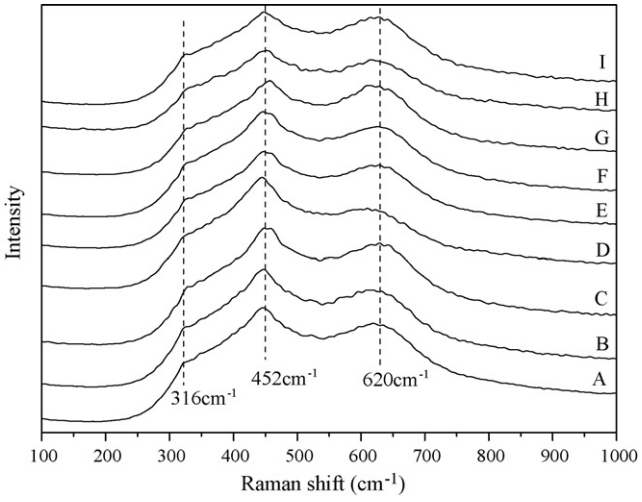

Fig. 5. Raman spectra of (A) CZ (8.6; 25; 250); (B) CZ (9.0; 25; 250); (C) CZ (9.5; 25; 250); (D) CZ (10.0; 25; 250); (E) CZ (9.5; 40; 250); (F) CZ (9.5; 60; 250); (G) CZ (9.5; 25; 170); (H) CZ (9.5; 25; 200); (I) CZ (9.5; 25; 230).

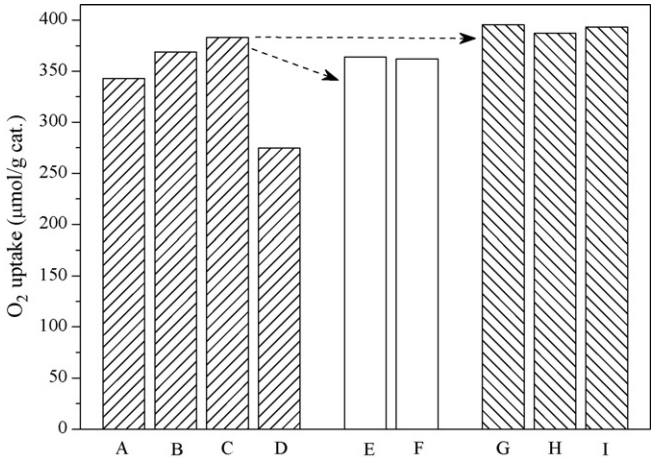

Fig. 6. OSCC values at 300 °C: (A) CZ (8.6; 25; 250); (B) CZ (9.0; 25; 250); (C) CZ (9.5; 25; 250); (D) CZ (10.0; 25; 250); (E) CZ (9.5; 40; 250); (F) CZ (9.5; 60; 250); (G) CZ (9.5; 25; 170); (H) CZ (9.5; 25; 200); (I) CZ (9.5; 25; 230).

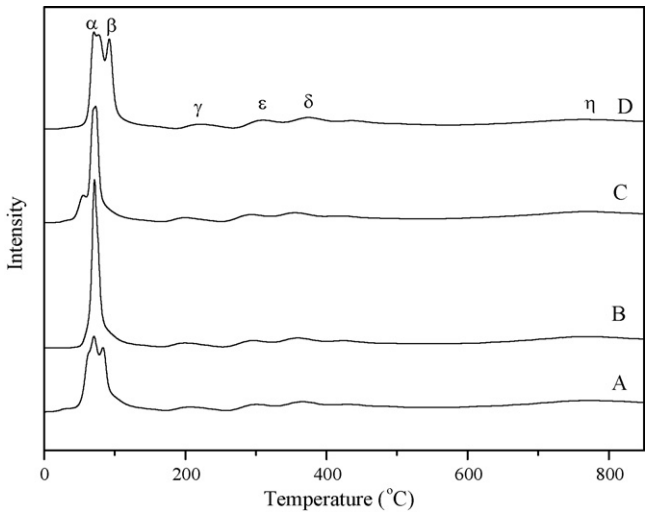

Fig. 7. TPR profiles of catalysts: (A) Pd/CZ (8.6; 25; 250); (B) Pd/CZ (9.0; 25; 250); (C) Pd/CZ (9.5; 25; 250); (D) Pd/CZ (10.0; 25; 250).

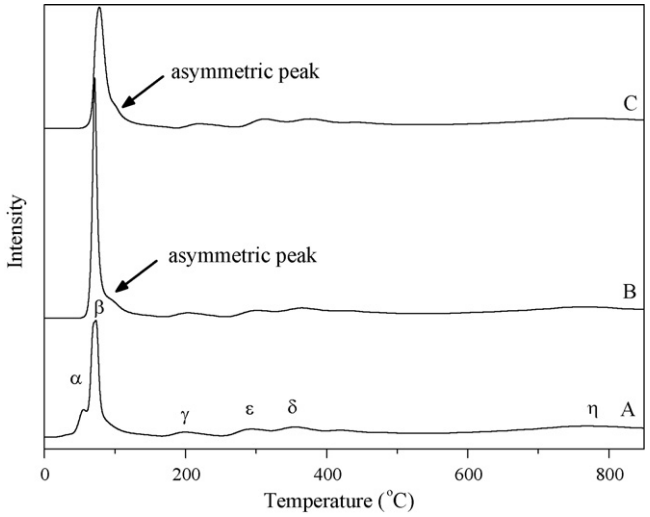

Fig. 8. TPR profiles of catalysts: (A) Pd/CZ (9.5; 25; 250); (B) Pd/CZ (9.5; 40; 250); (C) Pd/CZ (9.5; 60; 250).

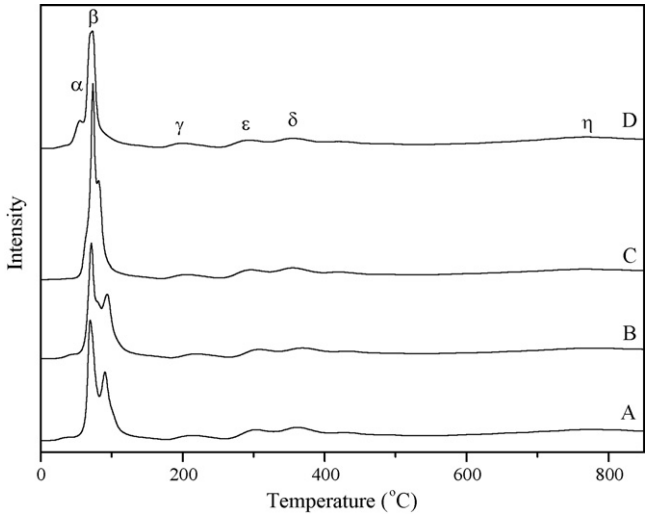

Fig. 9. TPR profiles of catalysts: (A) Pd/CZ (9.5; 25; 170); (B) Pd/CZ (9.5; 25; 200); (C) Pd/CZ (9.5; 25; 230); (D) Pd/CZ (9.5; 25; 250).

the α peak is ascribed to the reduction of highly dispersed PdO species and the β peak is corresponding to the reduction of stable PdO species having strong interaction with support. However, the total amount of the H_2 consumption of β peak is too large to be reasonable attributed to the reduction of noble metal oxides, as the amount of noble metal loaded is far too small (0.5 wt%). Jen et al. [40] have reported that the presence of noble metal is necessary for the reduction of $Ce_xZr_{1-x}O_2$ at lower temperatures. The oxidation of H_2 on the precious metal catalysts relies heavily on the spillover effect, which splits H_2 molecules into H atoms by precious metal. These highly reactive H atoms can easily reduce oxides by donating electrons at relatively low temperatures [33]. Therefore, we suggest that the presence of palladium facilitates the adsorption and spillover of hydrogen from the noble metal particles to the support, resulting in the interfacial Ce^{4+} reduction at low temperature [33,41]. The reduction peaks between 150 °C and 450 °C for all catalysts are very similar and typically characterized by the presence of more than one peak which is somehow overlapped (γ, ε, and δ). Its multimodal shape can be attributed to the reduction of oxygen species adsorbed on the oxygen vacancies which are generated by the formation of the solid solutions [42], the reduction of surface Ce^{4+} of the mixed oxide crystallites and the reduction with subsurface oxygen supplied from the bulk [10,41]. The reduction peak above 700 °C (peak η) is ascribed to the reduction of the bulk oxygen of supports [43], which is associated with the creation of oxygen vacancies and the migration of these vacancies into the bulk of the CZ solid solution.

As shown in Figs. 7–9, it can be seen that the reduction property of Pd/CZ catalyst is affected by the preparation condition of its support. Fig. 7 shows that the reduction temperature of β peak shifts downward from 84 °C to 71 °C when the pH is controlled from 8.6 to 9.5. Moreover, for the Pd/CZ (9.0; 25; 250) catalyst, only one peak appears below 150 °C, attributing to the downward shifting of the β peak and the mergence of α and β peak. We can also see that the Pd/CZ (9.5; 25; 250) catalyst exhibits the lowest reduction temperature of α peak (53 °C), which indicates that the catalyst supported on CZ (9.5; 25; 250) presents the best reduction behavior. For the Pd/CZ (10; 25; 250) catalyst, the intensity of α peak is obviously stronger than those of other catalysts, indicating that more palladium oxide exists as highly dispersed state on support. It is possibly due to the highest surface area of CZ (10; 25; 250) support (148.5 m^2/g). On the other hand, for the Pd/CZ (10; 25; 250) catalyst, the temperature of α and β peak shifts upward to 73 °C and 93 °C. This suggests that the catalyst reduction behavior is deteriorated when the pH is further increased from 9.5 to 10.0. Fig. 8 displays the TPR profiles of the catalysts supported on CZ prepared at different aging temperatures. It is worth noting that with the increasing of aging temperature, the reduction temperature of α peak shifts obviously to higher temperature. This results in the mergence of α and β peak for Pd/CZ (9.5; 40; 250) and Pd/CZ (9.5; 60; 250) catalysts, which can be seen by the asymmetric phenomena of the peak below 150 °C. The reduction behavior of catalyst supported on CZ prepared at different drying temperatures is presented in Fig. 9. It could be observed that the intensity of α peak is in good agreement with the surface area of its support. For instance, the strongest intensity of α peak is observed for Pd/CZ (9.5; 25; 230) catalyst due to its highest surface area of support (129.6 m^2/g). Moreover, the Pd/CZ (9.5; 25; 170) and Pd/CZ (9.5; 25; 200) catalysts present similar reduction behavior in the whole temperature range. Interestingly, it should be noted that the catalyst supported on CZ dried under supercritical alcohol exhibits the best reduction property with the lowest reduction temperature of α and β peak.

Based on the above outcomes, we suggest that the reduction property of Pd/CZ catalyst is significantly affected by the synthesis

condition of its support. It should be pointed out that the quantity of highly dispersed palladium oxide is certainly related to the surface area of its support. Specifically, the Pd/CZ (9.5; 25; 250) catalyst exhibits the best reduction behavior with the lowest reduction temperature among all of the catalyst.

3.6. Three-way catalytic activity

Fig. 10 presents the conversion of HC, CO, NO and NO_2 over Pd-only catalyst supported on CZ prepared at different drying temperature. The difference in temperature of T_{50} (the temperature required to attain 50% conversion) and T_{90} (the temperature required to attain 90% conversion) over different catalysts is shown in Table 3. As shown in Fig. 10, Pd/CZ (9.5; 25; 170) and Pd/CZ (9.5; 25; 200) exhibit the similar catalytic activity for the elimination of four species. This behavior could be correlated with the fact that the characteristics are nearly identical for these two catalysts as well as the corresponding supports. After further increasing the drying temperature of the support, Pd/CZ (9.5; 25; 230) catalyst exhibits slightly increasing activities and lower T_{50} and T_{90} compared to those of Pd/CZ (9.5; 25; 200) catalyst. Furthermore, Pd/CZ (9.5; 25; 250) catalyst exhibits the best catalytic activity for all of the reactants, especially for HC and NO elimination. For example, compared to Pd/CZ (9.5; 25; 170), a decrease in the T_{50} temperature of 27/26 °C is detected in the HC/NO elimination reactions over Pd/CZ (9.5; 25; 250). We suggest that there are two possible reasons: (i) Compared to the supports dried between 170 °C and 230 °C, CZ (9.5; 25; 250) exhibits the largest average pore size (20.42 nm) and pore volume (0.69 cm^3/g), which is more suitable for the support employed in high space velocity conditions; (ii) The catalyst supported on CZ (9.5; 25; 250) exhibits the best reduction behavior, which suggests that the catalytic activity may be related to the reducibility of PdO species, and the higher the reducibility of the PdO species, the higher the catalytic activities [44].

Table 3 also shows the effect of aging temperature and pH on the catalytic activity. It is concluded that the catalytic activity is decreased with increasing of aging temperature during synthesis of CZ. As mentioned above, the particle size of CZ is increased obviously when the aging temperature increases from 25 °C to 60 °C. Thus, one possible reason for the best catalytic activity of Pd/CZ (9.5; 25; 250) is the fine particle size of its support. Other reasons are related to the best reduction property of catalyst and the highest OSCC of CZ (9.5; 25; 250). Surface oxygen and oxygen vacancies seem to be involved in the catalytic improvement. The enhancement of the oxygen ion mobility can promote redox properties and oxygen diffusion through the catalyst, which further improves the activity [45]. From Table 3, it can also be seen that the difference of T_{50} and T_{90} is not distinguished clearly between Pd/CZ (8.6; 25; 250) and Pd/CZ (9.0; 25; 250). The Pd/CZ (9.5; 25; 250) catalyst exhibits the best catalytic activity, corresponding to the decrease of the light-off temperature and the promotion of the full conversion. On the contrary, when the pH is controlled at 10.0, the negative influence on the catalytic activity can be seen, especially for the increase in the T_{50} temperature of NO elimination reaction. It should be pointed out that the catalytic activity has no direct correlation with surface areas. Although CZ (10.0; 25; 250) possesses the highest surface area, it exhibits the lowest activities for all reactant. The smallest pore size and the lowest OSCC value of support together with the worst reducibility of catalyst result in the decrease of catalytic activity of Pd/CZ (10.0; 25; 250). From the above discussion, we have concluded that the catalytic activity of Pd/CZ is closely related to its reducibility and the structure, pore size distribution and OSCC of support.

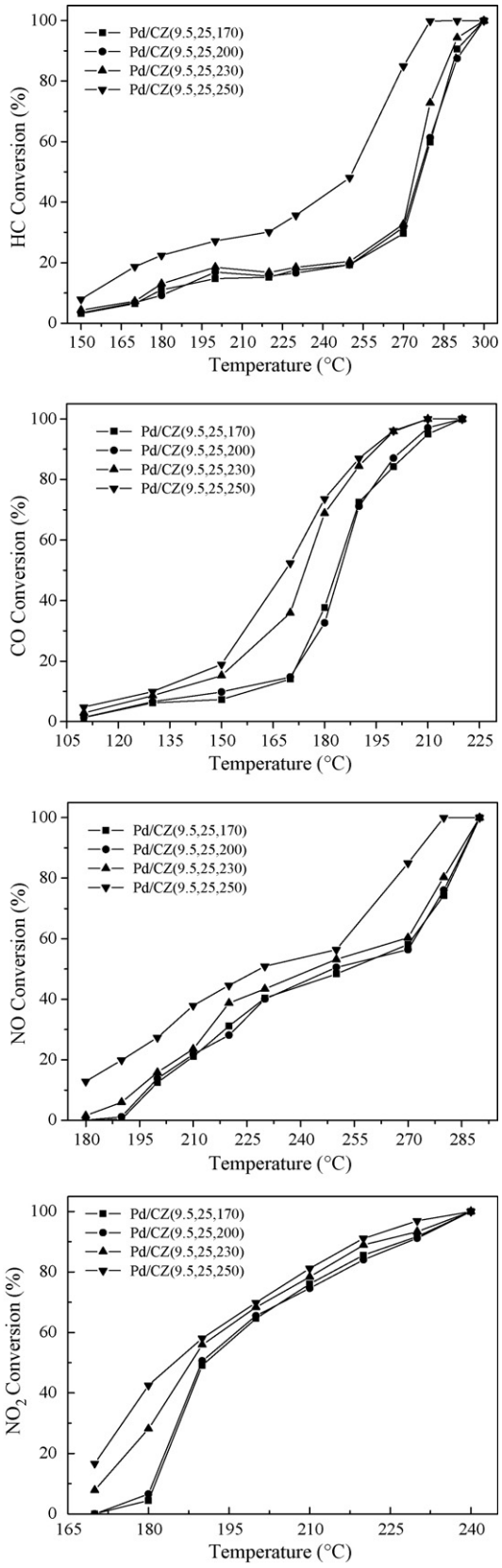

Fig. 10. Catalytic activities of HC, CO, NO and NO_2 over Pd-only catalyst supported on CZ prepared by different drying temperature.

Table 3
T_{50}, T_{90} of HC, CO, NO and NO_2 over different catalysts.

Catalyst	T_{50} (°C)				T_{90} (°C)			
	HC	CO	NO	NO_2	HC	CO	NO	NO_2
Pd/CZ (9.5; 25; 170)	277	184	254	191	290	205	286	228
Pd/CZ (9.5; 25; 200)	276	185	249	190	292	203	286	228
Pd/CZ (9.5; 25; 230)	274	174	244	188	288	195	285	223
Pd/CZ (9.5; 25; 250)	250	168	228	185	274	193	274	219
Pd/CZ (9.5; 40; 250)	253	176	233	188	279	201	274	218
Pd/CZ (9.5; 60; 250)	255	179	241	192	281	204	275	219
Pd/CZ(8.6; 25; 250)	253	184	237	190	275	204	274	225
Pd/CZ (9.0; 25; 250)	252	183	234	190	275	204	274	225
Pd/CZ (10.0; 25; 250)	256	188	250	201	277	210	276	230

4. Conclusions

The present work demonstrates the important role of synthesis condition in modifying both the textural and structural properties of $Ce_{0.67}Zr_{0.33}O_2$ and catalytic activity in a model TWC reaction. With the increase of aging temperature during precipitation, the crystallite size of CZ increases significantly, while the oxygen storage capacity complete drops and no notable effect on porosity of CZ is observed. Drying temperature has a significant influence on the porosity rather than on the structural properties of CZ. Moreover, the textural and structural properties of CZ are affected by the pH value during precipitation. Based on the above experimental facts, we speculate that the catalyst activity of Pd/CZ is affected by pore size distribution, the structural property and OSCC of its support as well as the reduction behavior of catalyst. It should be pointed out that CZ (9.5; 25; 250) support represents better textural and structural properties as well as OSCC promotion. Furthermore, Pd-only TWC supported on CZ (9.5; 25; 250) exhibits very low reduction temperature and the best catalytic activity.

Acknowledgements

We gratefully acknowledge the financial supports from the Ministry of Science and Technology of China (Nos. 2006AA060306, 2009AA064804).

References

[1] Z.Q. Zou, M. Meng, Y.Q. Zha, J. Alloys Compd. 470 (2009) 96–106.
[2] G.F. Li, Q.Y. Wang, B. Zhao, R.X. Zhou, J. Mol. Catal. A 326 (2010) 69–74.
[3] C.C. Chuang, H.I. Hsiang, J.S. Hwang, T.S. Wang, J. Alloys Compd. 470 (2009) 387–392.
[4] L.J. Meng, L.C. Liu, X.H. Zi, H.X. Dai, Z. Zhao, X.P. Wang, H. He, Front. Environ. Sci. Eng. China 4 (2010) 164–171.
[5] S. Bernal, G. Blanco, J.J. Calvino, J.C. Hernandez, J.A. Perez-Omil, J.M. Pintado, M.P. Yeste, J. Alloys Compd. 451 (2008) 521–525.
[6] S. Damyanova, B. Pawelec, K. Arishtirova, M.V. Martinez Huerta, J.L.G. Fierro, Appl. Catal. A 337 (2008) 86–96.
[7] G.Q. Xie, J.Q. Lu, H.Y. Zheng, X.J. Liu, M.F. Luo, X.N. Li, J. Alloys Compd. 493 (2010) 169–174.
[8] D. Terribile, A. Trovarelli, J. Llorca, C. de Leitenburg, G. Dolcetti, Catal. Today 43 (1998) 79–88.
[9] L.F. Chen, G. González, J.A. Wang, L.E. Noreña, A. Toledo, S. Castillo, M. Morán-Pineda, Appl. Surf. Sci. 243 (2005) 319–328.
[10] M. Thammachat, V. Meeyoo, T. Risksomboon, S. Osuwan, Catal. Today 68 (2001) 53–61.
[11] G.W. Graham, H.W. Jen, R.W. McCabe, A.M. Straccia, L.P. Hack, Catal. Lett. 67 (2000) 99–105.
[12] M. Fernádez-García, A. Martínez-Arias, A. Iglesis-Juez, A.B. Hungría, J.A. Anderson, J.C. Conesa, J. Soria, Appl. Catal. B 31 (2001) 39–50.
[13] F.C. Gennari, T. Montini, P. Fornasiero, J.J.A. Gamboa, Int. J. Hydrogen Energy 33 (2008) 3549–3554.
[14] A. Papavasiliou, A. Tsetsekou, V. Matsouka, M. Konsolakis, I.V. Yentekakis, N. Boukos, Appl. Catal. B 90 (2009) 162–174.
[15] X. Lu, X. Li, F. Chen, C. Ni, Z. Chen, J. Alloys Compd. 476 (2009) 958–962.
[16] M. Shen, J. Wang, J. Shang, Y. An, J. Wang, W. Wang, J. Phys. Chem. C 113 (2009) 1543–1551.
[17] L.D. Jadhav, M.G. Chourashiya, K.M. Subhedar, A.K. Tyagi, J.Y. Patil, J. Alloys Compd. 470 (2009) 383–386.
[18] S.T. Mukherjee, V. Bedekar, A. Patra, P.U. Sastry, A.K. Tyagi, J. Alloys Compd. 466 (2008) 493–497.
[19] A.V. Chadwick, S.L.P. Savin, J. Alloys Compd. 488 (2009) 1–4.
[20] J. Judes, V. Kamaraj, J. Sol–Gel Sci. Technol. 49 (2009) 159–165.
[21] J.C. Chen, W.C. Chen, Y.C. Tien, C.J. Shih, J. Alloys Compd. 496 (2010) 364–369.
[22] Z.L. Zhang, Y.X. Zhang, Z.G. Mu, P.F. Yu, X.Z. Ni, S.L. Wang, L.S. Zheng, Appl. Catal. B 76 (2007) 335–347.
[23] W.D. Wang, P.Y. Lin, Y.L. Fu, G.Y. Cao, Catal. Lett. 82 (2002) 19–27.
[24] B.M. Reddy, P. Bharali, P. Saikia, G. Thrimurthulu, Y. Yamada, T. Kobayashi, Ind. Eng. Chem. Res. 48 (2009) 453–462.
[25] J.A. Wang, L.F. Chen, M.A. Valenzuela, A. Montoya, J. Salmones, P.D. Angel, Appl. Surf. Sci. 230 (2004) 34–43.
[26] Z.L. Wei, H.M. Li, X.Y. Zhang, S.H. Yan, Z. Lv, Y.Q. Chen, M.C. Gong, J. Alloys Compd. 455 (2008) 322–326.
[27] J.X. Guo, D.D. Wu, L. Zhang, M.C. Gong, M. Zhao, Y.Q. Chen, J. Alloys Compd. 460 (2008) 485–490.
[28] L.N. Ikryannikova, A.A. Aksenov, G.L. Markaryan, G.P. Murav'eva, B.G. Kostyuk, A.N. Kharlanov, E.V. Lunina, Appl. Catal. A 210 (2001) 225–235.
[29] S. Damyanova, B. Pawelec, K. Arishtirova, M.V.M. Huerta, J.L.G. Fierro, Appl. Catal. A 337 (2008) 86–96.
[30] S. Pengpanich, V. Meeyoo, T. Rirksomboon, K. Bunyakiat, Appl. Catal. A 234 (2002) 221–233.
[31] S. Letichevsky, C.A. Tellez, R.R. de Avillez, M.I.P. da Silva, M.A. Fraga, L.G. Appel, Appl. Catal. B 58 (2005) 203–210.
[32] R. Si, Y.W. Zhang, S.J. Li, B.X. Lin, C.H. Yan, J. Phys. Chem. B 108 (2004) 12481–12488.
[33] J. Fan, X.D. Wu, X.D. Wu, Q. Liang, R. Ran, D. Weng, Appl. Catal. B 81 (2008) 38–48.
[34] A.I. Kozlov, D.H. Kim, A. Yezerets, P. Andersen, H.H. Kung, M.C. Kung, J. Catal. 209 (2002) 417–426.
[35] P. Fornasiero, G. Balducci, R. Di Monte, J. Kašpar, V. Sergo, G. Gubitosa, A. Ferrero, M. Graziani, J. Catal. 164 (1996) 173–183.
[36] P. Fornasiero, R. Di Monte, G.R. Rao, J. Kašpar, S. Meriani, A. Trovarelli, M. Graziani, J. Catal. 151 (1995) 168–177.
[37] B.K. Cho, J. Catal. 131 (1991) 74–87.
[38] E. Mamontov, R. Brezny, M. Koranne, T. Egami, J. Phys. Chem. B 107 (2003) 13007–13014.
[39] B. Zhao, G.F. Li, C.H. Ge, Q.Y. Wang, R.X. Zhoua, Appl. Catal. B 96 (2010) 338–349.
[40] H.W. Jen, G.W. Graham, W. Chun, R.W. McCabe, J.P. Cuif, S.E. Deutsch, O. Touret, Catal. Today 50 (1999) 309–328.
[41] H. He, H.X. Dai, L.H. Ng, K.W. Wong, C.T. Au, J. Catal. 206 (2002) 1–13.
[42] W.J. Shan, Z.C. Feng, Z.L. Li, J. Zhang, W.J. Shen, C. Li, J. Catal. 228 (2004) 206–217.
[43] X.D. Wu, J. Fan, R. Ran, J. Yang, D. Weng, J. Alloys Compd. 395 (2005) 135–140.
[44] R.X. Zhou, B. Zhao, B.H. Yue, Appl. Surf. Sci. 254 (2008) 4701–4707.
[45] J.R. González-Velasco, M.A. Gutiérrez-Ortiz, J.L. Marc, J.A. Botas, M.P. Gonzá lez-Marcos, G. Blanchard, Ind. Eng. Chem. Res. 39 (2000) 272–276.